Stanford Exploration Project, Report 111, June 9, 2002, pages 81–99

Wave-equation migration velocity analysis beyond the Born approximation

Paul Sava and Sergey Fomel[1]

ABSTRACT

The Born approximation is based on the assumption of small slowness perturbation. We investigate the limits of the Born approximation when applied to wave-equation migration velocity analysis and propose two new schemes which allow for larger slowness anomalies, while improving accuracy and increasing stability. The new schemes are based on linearizations of exponential functions using bilinear and implicit approximations, rather than the (Born) explicit approximation. We demonstrate the feasibility of our new operators on a synthetic example with highly variable background and strong slowness anomalies.

INTRODUCTION

Migration velocity analysis based on downward-continuation methods, commonly referred to as *wave-equation migration velocity analysis* (WEMVA), is a promising technique which has become an active area of research over the recent years (Biondi and Sava, 1999; Sava and Biondi, 2000, 2001). The main idea of WEMVA is to use downward-continuation operators not only for migration, but also for migration velocity analysis. This is in contrast with other techniques which use downward-continuation for migration but traveltime-based techniques for migration velocity analysis (Clapp, 2001; Liu et al., 2001; Mosher et al., 2001).

The main benefits of WEMVA are identical to the benefits of downward-continuation migration methods versus the more common Kirchhoff methods. Among these benefits, the most important are the accurate handling of complex wavefields, characterized by multipathing, and the band-limited nature of the imaging process, which can handle sharp velocity variations much better than traveltime-based methods (Woodward, 1992). The areas of complex geology are those where WEMVA is expected to provide the largest benefits.

The problem with WEMVA is that, in its simplest form, it is based on the Born approximation of the wavefield in the perturbation region. This leads to severe limitations of the magnitude and size of the anomalies that can be resolved, which means that, in principle, it cannot operate successfully in the regions of high complexity where it is needed most.

The limitations imposed by the Born approximation can be partially circumvented by spe-

[1]**email:** paul@sep.stanford.edu, fomel@math.lbl.gov

cial ways of creating the image perturbation in connection with residual migration (Sava and Biondi, 2001). This process of creating Born-compliant image perturbations is not the ideal strategy, since it closely links a highly accurate method, wavefield-continuation, to a less accurate method, Stolt residual migration.

In this paper, we introduce a new method of linearization designed to overcome the limitations imposed by the Born approximation. Our method is based on linearizations of the exponential function containing the slowness perturbation using more accurate approximations than Born linearization. The resulting operator is more accurate and also more stable in areas of high contrast, at a cost that is practically identical to the one of the Born linearized operator.

This paper is organized as follows: in the next two sections we review the theory of downward-continuation and wave-equation MVA using the Born approximation; then, we introduce the new operators and analyze their meaning in the general context of non-linear optimization; and finally, we present a synthetic example that demonstrates the features of our new method.

DOWNWARD-CONTINUATION MIGRATION

In migration by downward-continuation, the wavefield at depth $z+\Delta z$, $\mathcal{W}(z+\Delta z)$, is obtained by phase-shift from the wavefield at depth z, $\mathcal{W}(z)$.

$$\mathcal{W}(z+\Delta z) = \mathcal{W}(z)\, e^{-ik_z \Delta z}. \tag{1}$$

This equation corresponds to the analytical solution of the ordinary differential equation

$$\mathcal{W}'(z) = -ik_z \mathcal{W}(z), \tag{2}$$

where the $'$ sign represents a derivative with respect to the depth z.

We can consider that the depth wavenumber (k_z) depends linearly, through a Taylor series expansion, on its value in the reference medium (k_{z_r}) and the laterally varying slowness in the depth interval from z to $z+\Delta z$, $s(x,y,z)$

$$k_z \approx k_{z_r} + \left.\frac{dk_z}{ds}\right|_{s=s_r} (s-s_r), \tag{3}$$

where s_r represents the constant slowness associated with the depth slab between the two depth intervals, and $\left.\frac{dk_z}{ds}\right|_{s=s_r}$ represents the derivative of the depth wavenumber with respect to the reference slowness and which can be implemented in many different ways (Sava, 2000). The wavefield downward-continued through the *background* slowness $s_b(x,y,z)$ can, therefore, be written as

$$\mathcal{W}_b(z+\Delta z) = \mathcal{W}(z)\, e^{-i\left[k_{z_r} + \left.\frac{dk_z}{ds}\right|_{s=s_r}(s_b-s_r)\right]\Delta z}, \tag{4}$$

from which we obtain that the full wavefield $\mathcal{W}(z+\Delta z)$ depends on the background wavefield $\mathcal{W}_b(z+\Delta z)$ through the relation

$$\mathcal{W}(z+\Delta z) = \mathcal{W}_b(z+\Delta z)\, e^{-i\,\frac{dk_z}{ds}\Big|_{s=s_r}\Delta s\Delta z}, \tag{5}$$

where Δs represents the difference between the true and background slownesses $\Delta s = s - s_b$.

BORN WAVE-EQUATION MVA

We define the *wavefield perturbation* $\Delta\mathcal{W}(z+\Delta z)$ as the difference between the wavefield propagated through the medium with correct velocity $\mathcal{W}(z+\Delta z)$ and the wavefield propagated through the background medium $\mathcal{W}_b(z+\Delta z)$. With these definitions, we can write

$$\Delta\mathcal{W}(z+\Delta z) = \mathcal{W}(z+\Delta z) - \mathcal{W}_b(z+\Delta z), \tag{6}$$

or

$$\Delta\mathcal{W}(z+\Delta z) = \mathcal{W}_b(z+\Delta z)\left[e^{-i\,\frac{dk_z}{ds}\Big|_{s=s_r}\Delta s\Delta z} - 1\right]. \tag{7}$$

Equation (7) represents the foundation of the wave-equation migration velocity analysis method (Biondi and Sava, 1999). The major problem with Equation (7) is that the wavefield $\Delta\mathcal{W}$ and slowness perturbations Δs are not related through a linear relation, therefore, for inversion purposes, we need to further approximate it by linearizing the equation around the reference slowness (s_r)

Biondi and Sava (1999) choose to linearize Equation (7) using the Born approximation ($e^{i\phi} \approx 1 + i\phi$), from which the WEMVA equation becomes

$$\Delta\mathcal{W}(z+\Delta z) = \mathcal{W}_b(z+\Delta z)\left[-i\,\frac{dk_z}{ds}\Big|_{s=s_r}\Delta s\Delta z\right]. \tag{8}$$

The problem with the Born linearization, Equation (8), is that it is is based on an assumption of small phase perturbation,

$$1 + i\phi \approx \lim_{\phi\to 0} e^{i\phi}$$

which mainly translates into small slowness perturbations. This fact is more apparent if we recall that the linearization $e^{i\phi} \approx 1 + i\phi$ corresponds to an explicit numerical solution of the differential equation (2), a numerical solution which is notoriously unstable unless precautions are taken to consider small propagation steps. The main consequence of the limitations imposed by the Born approximation is that WEMVA can only consider small perturbations in the slowness model, which are likely too small relative to the demands of real problems. Since non-linear inversion is still not feasible for large size problems like the ones typical for seismic imaging, we seek other ways of linearizing Equation (7) which would still enable us to solve our inversion problem within the framework of linear optimization theory.

HIGHER ACCURACY LINEARIZATIONS

As noted earlier, the approximation

$$e^{i\phi} \approx 1 + i\phi \tag{9}$$

corresponds to an *explicit* numerical solution to the differential equation (2). However, this is neither the only possible solution, nor the most accurate, and furthermore it is only conditionally stable.

We can, however, solve Equation (2) using other numerical schemes. Two possibilities are *implicit* numerical solutions, where we approximate

$$e^{i\phi} \approx \frac{1}{1 - i\phi}, \tag{10}$$

or *bilinear* numerical solutions, where we approximate

$$e^{i\phi} \approx \frac{2 + i\phi}{2 - i\phi}. \tag{11}$$

Equations (9) and (10) are first order, but Equation (11) is second order accurate as a function of the phase ϕ. Numerical schemes based on Equation (9) are conditionally stable, but numerical schemes based on Equations (10) and (11) are unconditionally stable.

In the context of partial differential equations, the bilinear approximation (11) is known under the name of Crank-Nicolson and has been extensively used in migration by downward-continuation using the paraxial wave equation (Claerbout, 1985). Figures 1 and 2 compare the approximations in Equations (9), (10) and (11) as a function of phase. Both the explicit and implicit solutions lead to errors in amplitude and phase, while the bilinear solution leads just to errors in phase (Figure 2).

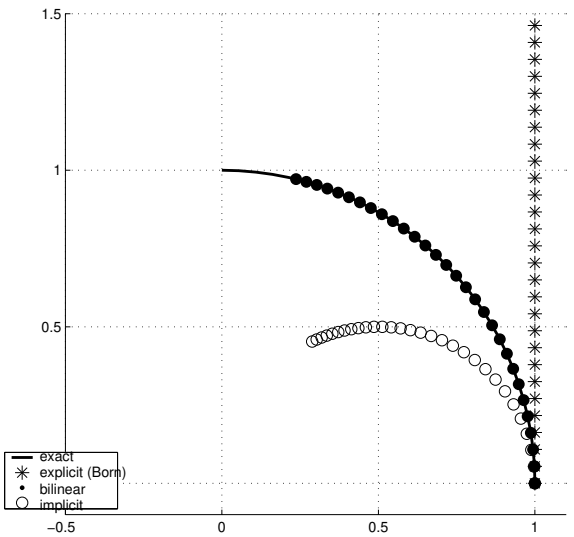

Figure 1: Explicit, bilinear and implicit approximations plotted on the unit circle. The solid line corresponds to the exact exponential solution. paul1-unit [NR]

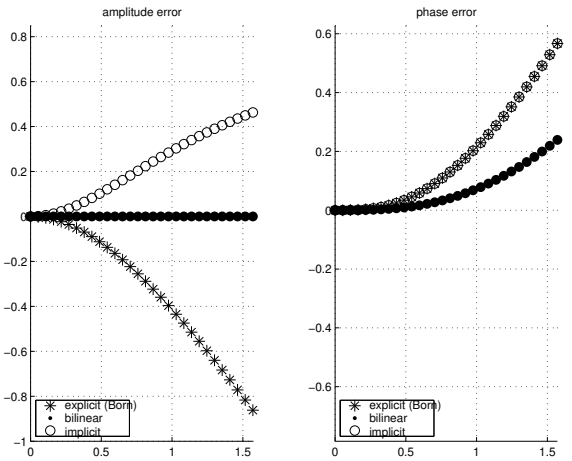

Figure 2: Amplitude and phase errors for the explicit, bilinear and implicit approximations. paul1-exap [NR]

If, for notation simplicity, we define

$$\beta = -i \left. \frac{dk_z}{ds} \right|_{s=s_r} \Delta z, \tag{12}$$

the WEMVA equation (7) can be written as

$$\Delta \mathcal{W} = \mathcal{W}_b \left[e^{\beta \Delta s} - 1 \right], \tag{13}$$

and so the linearizations corresponding to the explicit, bilinear and implicit solutions respectively become

$$\begin{aligned} \Delta \mathcal{W} &\approx \mathcal{W}_b \beta \Delta s \\ &\approx \mathcal{W}_b \frac{2\beta \Delta s}{2 - \beta \Delta s} \\ &\approx \mathcal{W}_b \frac{\beta \Delta s}{1 - \beta \Delta s} \end{aligned} \tag{14}$$

Aparently, just the first equation in (14) provides a linear relationship between $\Delta \mathcal{W}$ and Δs. However, a simple re-arrangement of terms leads to

$$\begin{aligned} \Delta \mathcal{W} &\approx \beta \left[\mathcal{W}_b \right] \Delta s \\ &\approx \beta \left[\mathcal{W}_b + \frac{1}{2} \Delta \mathcal{W} \right] \Delta s \\ &\approx \beta \left[\mathcal{W}_b + \Delta \mathcal{W} \right] \Delta s. \end{aligned} \tag{15}$$

For MVA, both the background ($\mathcal{W}_b$) and perturbation wavefields ($\Delta \mathcal{W}$) are known, so it is not a problem to incorporate them in the linear operator. In any of the cases described in Equation (15), the approximations can be symbolically written using the fitting goal

$$\mathbf{d} \approx \mathbf{L}\mathbf{m}, \tag{16}$$

where the data **d** is the wavefield perturbation, and the model **m** is the slowness perturbation. The same operator **L** is used for inversion in all situations, the only change being in the wavefield that is fed into the linear operator. Therefore, the new operators are not more expensive than the Born operator.

All linear relationships in Equation (15) belong to a family of approximations of the general form

$$\Delta \mathcal{W} \quad \approx \quad \beta \left[\mathcal{W}_b + \xi \, \Delta \mathcal{W} \right] \Delta s. \tag{17}$$

The various approximations can be obtained using appropriate values for the parameter $\xi = 0 \ldots 1$. All forms of Equation (17), however, are approximations to the exact non-linear relation (13), therefore they are all likely to break for large values of the phase, or equivalently large values of the slowness perturbation or frequency. Nevertheless, these approximations enable us to achieve higher accuray in slowness estimation as compared to the simple Born approximation.

An interesting comparison can be made between the extreme members of the sequence given by Equation (17): for $\xi = 0$ we use the background wavefield $\mathcal{W}_b$, and for $\xi = 1$ we use the full wavefield $\mathcal{W} = \mathcal{W}_b + \Delta \mathcal{W}$. The physics of scattering would recommend that we use the later form, since the scattered wavefield ($\Delta \mathcal{W}$) is generated by the total wavefield ($\mathcal{W}$), and not by an approximation of it ($\mathcal{W}_b$), thus naturally accounting for multiple scattering effects. The later situation also corresponds to what is known in the scattering literature as *wavefield renormalization* (Wang, 1997). The details of these ideas and their implications remain open for future research.

Finally, we note that Equation (17) cannot be used for forward modeling of the wavefield perturbations $\Delta \mathcal{W}$, except for the particular case $\xi = 0$, since the output quantity is contained in the operator itself. However, we can use this equation for inversion for any choice of the parameter ξ.

NEWTON'S METHOD AND WEMVA

One can also consider the problem of estimating the slowness field from wavefields using WEMVA in the general non-linear inversion framework.

In particular, if $\mathcal{W}(z + \Delta z)$ is the upgpoing wavefield at the bottom of a layer and $\mathcal{W}(z)$ is the upgoing wavefield at the top of the layer, the layer slowness s is constrained by the nonlinear equation

$$F[s] = P[s] \, \mathcal{W}(z + \Delta z) - \mathcal{W}(z) = 0 \,, \tag{18}$$

where $P[s] = e^{i k_z [s]}$ is the wave propagation operator.

The Newton method applied to equation (18) amounts to inversion of the linear system

$$F'[s_k](s_{k+1} - s_k) = -F[s_k] \,, \tag{19}$$

where k is the nonlinear iteration counter (the iteration starts with some a priori slowness model s_0), and $F'[s]$ is the Fréchet derivative of the wave propagation operator. Since $F[s]$ is complex-valued, we can multiply both sides of system (19) by the adjoint (complex-conjugate) operator $F'[s_k]^T$ to obtain the purely real system

$$\begin{aligned} F'[s_k]^T\, F'[s_k]\,(s_{k+1}-s_k) &= -F'[s_k]^T\, F[s_k] \\ \left(R'[s_k]^T\, R'[s_k]+I'[s_k]^T\, I'[s_k]\right)\,(s_{k+1}-s_k) &= -\left(R'[s_k]^T\, R[s_k]+I'[s_k]^T\, I[s_k]\right)\,, \end{aligned} \tag{20}$$

where $R[s]$ and $I[s]$ are the real and imaginary parts of $F[s]$. Algorithm (21) is equivalent to the Gauss-Newton method applied to the least-squares solution of

$$R[s] \approx 0\,, \tag{21}$$

$$I[s] \approx 0\,. \tag{22}$$

It is well-known that the Newton and Newton-Gauss methods possess fast convergence provided that the original estimate s_0 is sufficiently close to the solution. They may diverge otherwise. To guarantee convergence, the norm (spectral radius) of the Fréchet derivative $G'[s]$ for the operator

$$G[s] = s - \frac{R'[s]^T\, R[s]+I'[s]^T\, I[s]}{R'[s]^T\, R'[s]+I'[s]^T\, I'[s]} \tag{23}$$

must be strictly smaller than one in the vicinity of the solution that contains the starting value s_0. Convergence follows then from the contraction mapping theorem. The speed of convergence is higher for smaller norms.

It is important to realize that modifying the original nonlinear Equation (18) may change the convergence behavior and lead to faster convergence and wider convergence area. A particularly meaningful way to modify Equation (18) is to multiply it by $P[s]^{-\xi}$, where ξ is a scalar between 0 and 1. The modified equation takes the form

$$F_\xi[s] = P[s]^{-\xi}\, F[s] = P[s]^{1-\xi}\, \mathcal{W}(z+\Delta z) - P[s]^{-\xi}\, \mathcal{W}(z) = 0\,. \tag{24}$$

The case of $\xi = 0$ corresponds to the original system. Its linearization with the Newton method leads to the Born approximation. Analogously, the case of $\xi = 1$ corresponds to the implicit method: the two wavefields are compared at the bottom of the layer rather than at the top. The case of $\xi = 1/2$ leads to the bilinear method: both wavefields are continued to the middle of the layer for comparison. Many other intermediate results are possible,

Example

The simplest case to study analytically is that of vertically-incident waves in laterally homogeneous media. In this case, all operators become functions of the scalar variable s (unknown layer slowness). If, for a particular temporal frequency ω and the layer thickness Δz, we measure the slowness in units of $1/(\omega\,\Delta z)$, the wave continuation operator is simply the phase shift

$$P(s) = e^{i\,s}\,, \tag{25}$$

and the fundamental nonlinear equation takes the form

$$F_\xi(s) = \mathcal{W}(z+\Delta z)\, e^{i(1-\xi)s} - \mathcal{W}(z)\, e^{-i\xi s} = 0\,. \tag{26}$$

Noting that

$$\mathcal{W}(z) = \mathcal{W}(z+\Delta z)\, e^{i s^\star}\,, \tag{27}$$

where $s^\star$ is the true slowness, and that the convergence of Newton's method does not depend on scaling the equation by a constant, we can modify equation (26) to the simpler form

$$\hat{F}_\xi(s) = F_\xi(s)\,\frac{e^{(\xi-1)s^\star}}{\mathcal{W}(z+\Delta z)} = e^{i(1-\xi)\Delta s} - e^{-i\xi\Delta s} = 0\,, \tag{28}$$

where $\Delta s = s - s^\star$. The obvious solution of Equation (28) is $\Delta s = 0$. Our task is to find the convergence limits and their dependence on ξ.

After a number of algebraic and trigonometric simplifications, the operator G from equation (23) takes the form of the function

$$\hat{G}_\xi(s) = s - \frac{\sin(\Delta s)}{1-2(1-\xi)\xi+2(1-\xi)\xi\,\cos(\Delta s)} \tag{29}$$

Its derivative is

$$\hat{G}'_\xi(s) = 2\sin^2\left(\frac{\Delta s}{2}\right)\frac{1-2(1-x)x\,[3-2(1-x)x]-4(1-x)^2x^2\cos(\Delta s)}{[1-2(1-\xi)\xi+2(1-\xi)\xi\,\cos(\Delta s)]^2}\,. \tag{30}$$

The method will converge in the region around $\Delta s = 0$, where the absolute value of $\hat{G}'_\xi(s)$ is strictly smaller than one. This region (as a function of Δs and ξ) is plotted in Figure 3. We can see that the convergence region has a finite extent. Its width is the same for $\xi = 0$, $\xi = 1$, and $\xi = 1/2$. Indeed,

$$\hat{G}'_0(s) = \hat{G}'_1(s) = 2\sin^2\left(\frac{\Delta s}{2}\right) \tag{31}$$

and

$$\hat{G}'_{1/2}(s) = -\tan^2\left(\frac{\Delta s}{2}\right). \tag{32}$$

In both cases, the absolute value of the derivative is smaller than one if $\Delta s < \frac{\pi}{2}$. If we take $\omega = 2\pi \times 100\,\text{Hz}$ and $\Delta z = 10\,\text{m}$, then the convergence radius is $\Delta s = 0.25\,\text{s/km}$. At small Δz,

$$\hat{G}'_0(s) = \hat{G}'_1(s) \approx \frac{(\Delta s)^2}{2} \tag{33}$$

and

$$\hat{G}'_{1/2}(s) \approx \frac{(\Delta s)^2}{4}\,. \tag{34}$$

The convergence rate is of the same order (cubic) but faster in the case of the bilinear method ($\xi = 1/2$), because of the twice smaller constant. Here is an example of iterations starting with $s_0 = 2$ and converging to $s^\star = \pi$. The Born iteration:

$$\begin{aligned} s_1 &= 2.9093 \\ s_2 &= 3.13951 \\ s_3 &= 3.14159 \end{aligned}$$

The bilinear iteration:

$$\begin{aligned} s_1 &= 3.28419 \\ s_2 &= 3.14135 \\ s_3 &= 3.14159 \end{aligned}$$

A faster convergence can be achieved at some other values of ξ. Examining the Taylor series of $\hat{G}'_\xi(s)$ around $\Delta s = 0$:

$$\hat{G}'_\xi(s) \approx [1 - 6(1-\xi)\xi] \, \frac{(\Delta s)^2}{2} \, , \tag{35}$$

we find that the order of convergence is optimized for $\xi = \frac{1}{2} \pm \frac{\sqrt{3}}{6}$. In this case,

$$\hat{G}'_{1/2 \pm \sqrt{3}/6}(s) = \frac{4 \sin^4\left(\frac{\Delta s}{2}\right)}{[2 + \cos(\Delta s)]^2} \approx \frac{(\Delta s)^4}{36} \, , \tag{36}$$

and the convergence is fifth order! The example iterations with the optimal value of ξ are:

$$\begin{aligned} s_1 &= 3.12903 \\ s_2 &= 3.14159 \\ s_3 &= 3.14159 \end{aligned}$$

The radius of convergence with the optimal value of ξ is $\Delta s < \frac{2}{3}\pi$.

Of course, this analysis does not apply directly to the case of non-vertical wave propagation and laterally inhomogenous slowness fields. For reflection wavefields at multiple offsets, the symmetry between downward and upward continuation is broken, as is clear from the experimental results of this paper. However, the simple analysis points to the potential benefits of modifying the Born approximation in the wave-equation velocity estimation.

PHYSICAL INTERPRETATION

This section presents a brief physical interpretation of the various members of relation (17).

Consider that we have recorded two wavefields at the top and bottom of a depth slab: W_0, the wavefield at the top of the slab which has not propagated through the anomalous region;

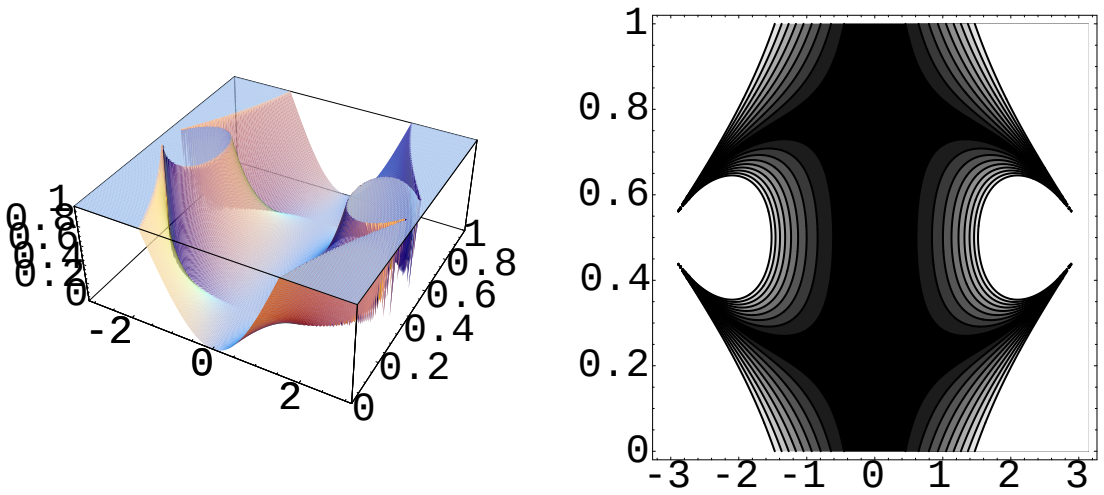

Figure 3: Convergence region for the Newton-Gauss method in the vertical plane-wave example. Left: 3-D projection. Right: contours. The non-white region on the right plot corresponds to the convergence area. Horizontal axis: Δs. Vertical axis: ξ. paul1-zo [NR]

W_1, the wavefield at the bottom of the slab which incorporates scattering effects caused by the slowness anomaly inside the slab. The goal of WEMVA is to extract the slowness perturbation Δs from W_0 and W_1.

We can imagine that the linearized process can be thought of as a succession of four steps.

1. Continuation of W_0 and W_1 to a level inside the slab where we can compare the two wavefields. This level can be either at the top, bottom or anywhere in between:

$$W_1 e^{-\xi k_z(s)} = W_0 e^{(1-\xi) k_z(s)} \tag{37}$$

   k_z represents the depth wavenumber and is a function of the arbitrary slowness inside any given depth slab, and $\xi = 0 \ldots 1$ is a scalar which defines where inside the slab we continue the two wavefields.

2. Linearization of W_0 and W_1 with respect to the slowness perturbation:

$$W_1 e^{-\xi k_z(s_0)}[1 - \xi\beta\Delta s] = W_0 e^{(1-\xi)k_z(s_0)}[1 + (1-\xi)\beta\Delta s], \tag{38}$$

   where β is the function defined in Equation (12).

3. Datuming of the linearized wavefields to the bottom of the slab:

$$\begin{aligned} W_1[1 - \xi\beta\Delta s] &= W_0[1 + (1-\xi)\beta\Delta s] e^{k_z(s_0)} && (39) \\ &= W_b[1 + (1-\xi)\beta\Delta s] && (40) \end{aligned}$$

4. Subtraction of the wavefield propagated through the perturbed medium from the wavefield propagated through the background medium:

$$\Delta W = W_1 - W_b = W_b \frac{\beta \Delta s}{1 - \xi \beta \Delta s} \tag{41}$$

All three cases in Equation (14) can be derived from Equation (41) as follows:

$$\xi = 0 \quad \rightarrow \quad \Delta W = W_b \beta \Delta s \tag{42}$$

$$\xi = \frac{1}{2} \quad \rightarrow \quad \Delta W = W_b \frac{2\beta \Delta s}{2 - \beta \Delta s} \tag{43}$$

$$\xi = 1 \quad \rightarrow \quad \Delta W = W_b \frac{\beta \Delta s}{1 - \beta \Delta s}. \tag{44}$$

EXAMPLES

We demonstrate the technique outlined in the preceding sections using a synthetic example. The model (Figure 4) consists of a body of high velocity incorporated in a background with strong but smooth lateral velocity variation.

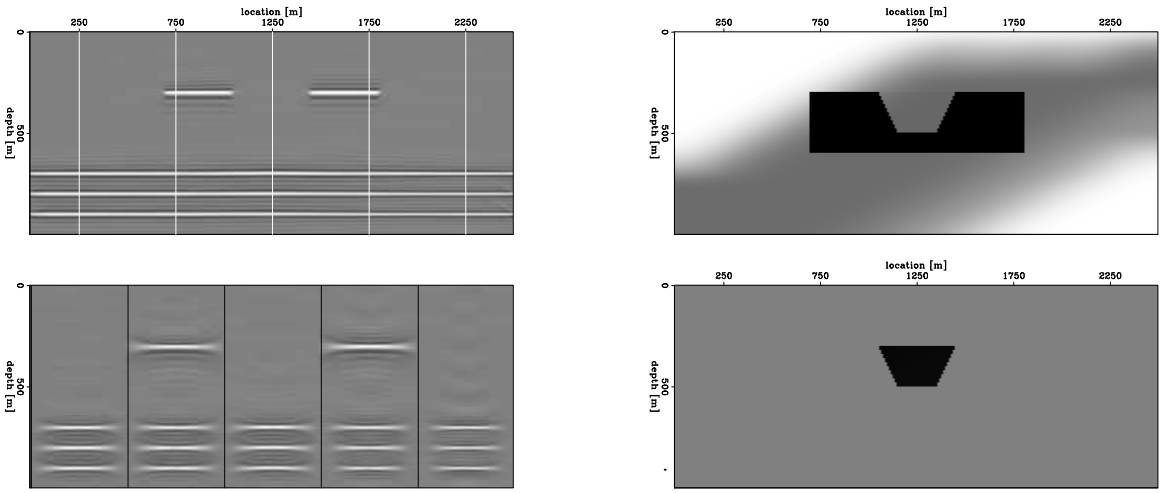

Figure 4: Synthetic model. Reflectivity model (top left) and a few angle-gathers corresponding to the vertical grid in the upper plot (bottom left). Background slowness model (top right) and slowness perturbation (bottom right). paul1-model [CR,M]

Our examples show the results of inversion for a regularized problem symbolically sumarized by the fitting goals:

$$\begin{aligned} \Delta R &\approx \mathbf{L} \Delta s \\ 0 &\approx \mathbf{A} \Delta s, \end{aligned} \tag{45}$$

where ΔR is the image perturbation, Δs is the corresponding slowness perturbation, $\mathbf{L}$ is one of the linearized WEMVA operators and $\mathbf{A}$ is a roughening operator, an isotropic Laplacian for our examples. After preconditioning (Claerbout, 1999), our fitting goals become

$$\begin{aligned} \Delta R &\approx \mathbf{L}\mathbf{A}^{-1}\Delta p, \\ 0 &\approx \Delta p \end{aligned} \tag{46}$$

where Δp represents the preconditioned Δs.

We also note that since the operator $\mathbf{L}$ is large, similar in size to a migration operator, we cannot implement it in-core, and therefore we have to use out-of-core optimization (Sava, 2001).

For our experiments, we generate two kinds of image perturbations.

- The first kind is created from a given slowness perturbation Δs using the linear operator in Equation (15). We refer to this type of image perturbation as *linear*, since it corresponds to the linearized Born operator. This type of image perturbation cannot be obtained in real applications, but serves as a reference when we investigate the Born approximation.
- The second kind is created by taking the difference of two images created using two slowness models ($\Delta R = R - R_o$). We refer to this type of image perturbation as *non-linear*, since it corresponds to the non-linear relation in Equation (7).

We analyze several examples where we change the magnitude of the slowness anomaly, but not its shape. We choose to test various magnitudes for the anomaly from 1% to 50% of the background slowness.

Figures 5, 7, 9, 11 show the image perturbations created by the slowness anomalies for the various levels of perturbation. In each figure, the left panels present the linear case, and the right panels the non-linear case. The top panels depict the stacked sections, and the bottom panels a few representative image gathers in the angle-domain (Sava and Fomel, 2000) corresponding to the locations of the vertical lines in the upper panels. For small values of the slowness perturbations, the two images should be similar, but for larger values we should see the image perturbation reaching and eventually breaking the Born approximation.

Figures 6, 8, 10, 12 present the results of inversion of the non-linear ΔR using the three WEMVA operators presented in the preceding section: the explicit (Born) operator (top), the bilinear operator (middle), and the implicit operator (bottom).

For the case of the small slowness perturbation (1%), the linear and non-linear image perturbations are very similar, as seen in Figure (5). The corresponding slowness anomaly obtained by inversion is well focused, confirming that, for this case, even the Born approximation is satisfactory, as suggested by the theory.

The larger anomaly of 5% of the background slowness shows the serious signs of breakdown for the Born approximation. For the case of the even larger slowness perturbation (20%),

the linear and non-linear image perturbations are not that similar anymore, indicating that we have already violated the limits of the Born approximation (Figure 9). Consequently, the inversion from the non-linear image perturbation using the Born operator blows-up. However, the WEMVA operators employing the bilinear and implicit approximations are still well-behaved, although the shape of the anomaly is slightly modified.

The case of the largest slowness anomaly (40%), bring us closer to the limits of both the bilinear and implicit approximations. Although neither has blown-up yet, the shape of the anomalies is somewhat altered.

CONCLUSIONS

In this paper, we investigate the limits of the Born approximation when applied to wave-equation migration velocity analysis. Experimentally we find that the Born approximation is only valid for small slowness anomalies, on the order of $1-2\%$ of the background slowness for an anomaly of the shape and size used in the example in this paper. These numbers, however, are model dependent, because we have to consider both the magnitude and size of the anomaly: a small anomaly of large magnitude can have a similar effect as a large anomaly of small magnitude.

Moving beyond the Born approximation involves one of the two solutions: we can either artificially create image perturbations that are compliant with this approximation (Sava and Biondi, 2001), or we can improve the WEMVA operator to better handle the non-linearity in the image perturbations, as presented in this paper. [2]

We propose two improved versions of the WEMVA operator which are more appropriate for the case of large/strong slowness anomalies. Our new operators involve linearizations using bilinear and implicit approximations to the exponential function. With the new operators, we not only improve accuracy but we also maintain stability of the inversion scheme at much higher values of the slowness anomalies, even in the order of 25% of the background.

Finally, we note that our new operators come at a cost which is practically no different than the cost of the Born-linearized operator, while improving its accuracy and stability.

REFERENCES

Biondi, B., and Sava, P., 1999, Wave-equation migration velocity analysis: SEP–**100**, 11–34.

Claerbout, J. F., 1985, Imaging the Earth's Interior: Blackwell Scientific Publications.

Claerbout, J., 1999, Geophysical estimation by example: Environmental soundings image enhancement: Stanford Exploration Project, `http://sepwww.stanford.edu/sep/prof/`.

[2]It appears that another possibility would be to use the Rytov approximation, and establish a linear relation between the slowness and phase perturbations. This method, however, is somewhat more problematic, since it may involve phase unwrapping of complex wavefields. It remains, however, an interesting area for future research.

Clapp, R. G., 2001, Geologically constrained migration velocity analysis: Ph.D. thesis, Stanford University.

Liu, W., Popovici, A., Bevc, D., and Biondi, B., 2001, 3-D migration velocity analysis for common image gathers in the reflection angle domain: 71st Annual Internat. Mtg., Soc. Expl. Geophys., Expanded Abstracts, 885–888.

Mosher, C., Jin, S., and Foster, D., 2001, Migration velocity analysis using angle image gathers: 71st Annual Internat. Mtg., Soc. Expl. Geophys., Expanded Abstracts, 889–892.

Sava, P., and Biondi, B., 2000, Wave-equation migration velocity analysis: Episode II: SEP–**103**, 19–47.

Sava, P., and Biondi, B., 2001, Born-compliant image perturbation for wave-equation migration velocity analysis: SEP–**110**, 91–102.

Sava, P., and Fomel, S., 2000, Angle-gathers by Fourier Transform: SEP–**103**, 119–130.

Sava, P., 2000, A tutorial on mixed-domain wave-equation migration and migration velocity analysis: SEP–**105**, 139–156.

Sava, P., 2001, `oclib`: An out-of-core optimization library: SEP–**108**, 199–224.

Wang, G. Y., 1997, Wave scattering and diffraction tomography in complex media: Ph.D. thesis, Stanford University.

Woodward, M. J., 1992, Wave-equation tomography: Geophysics, **57**, no. 01, 15–26.

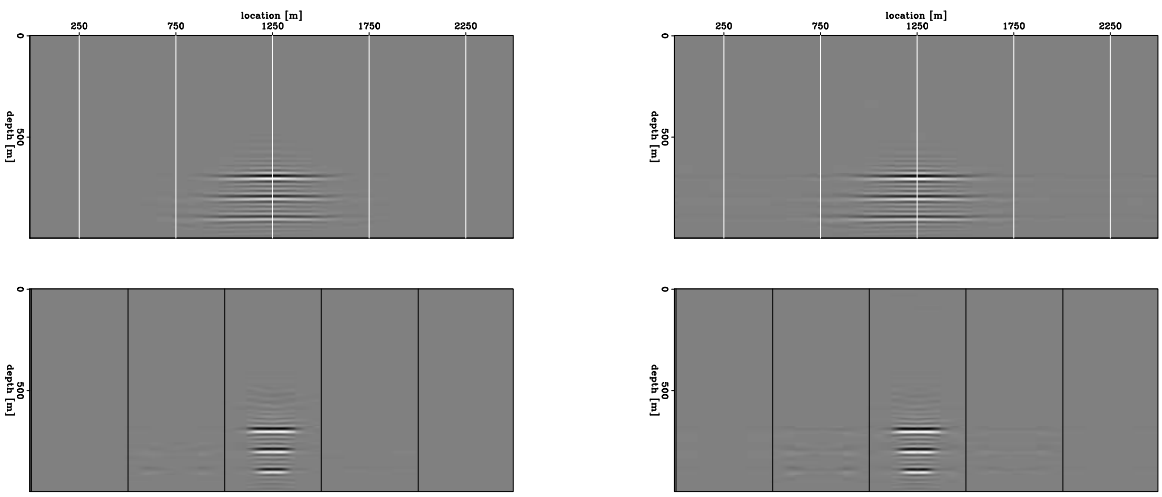

Figure 5: Anomaly of 1%: linear and non-linear image perturbations (left/right); zero offset section (top) and selected angle-gathers (bottom) corresponding to the locations of the vertical lines in the upper panel. Large differences between the linear and non-linear image perturbations indicate situations in which we violate the Born approximation. paul1-01.perturbation [CR,M]

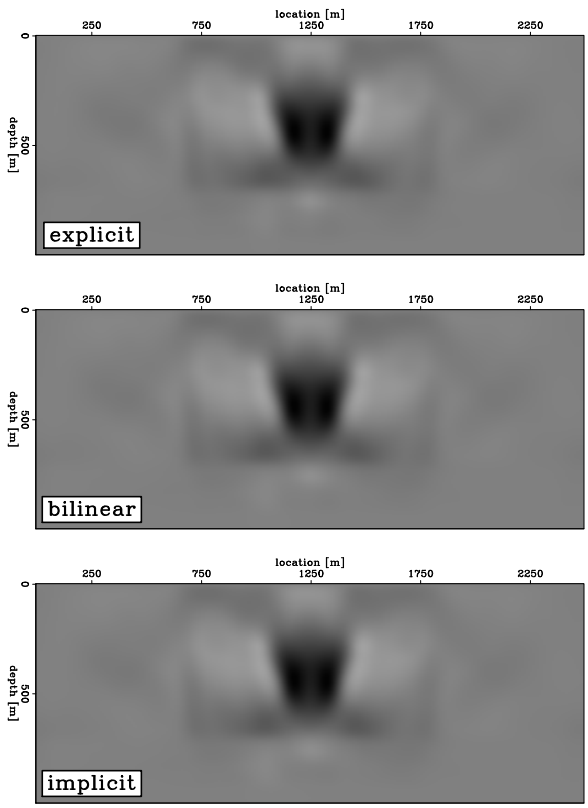

Figure 6: Anomaly of 1%: inversion from the non-linear image perturbation (7) using the explicit (top), bilinear (middle) and implicit (bottom) WEMVA operators. paul1-01.inversion [CR,M]

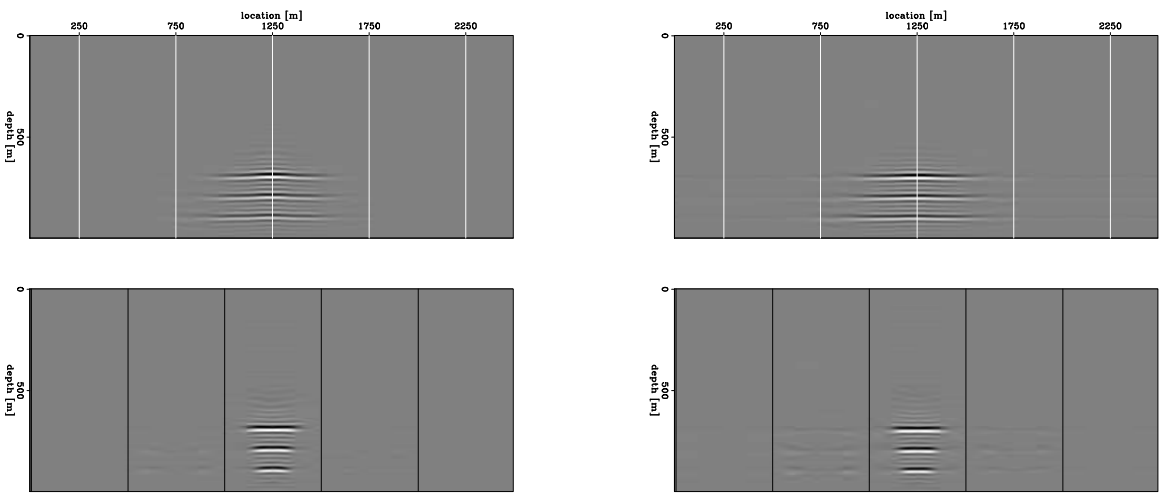

Figure 7: Anomaly of 5%: linear and non-linear image perturbations (left/right); zero offset section (top) and selected angle-gathers (bottom) corresponding to the locations of the vertical lines in the upper panel. Large differences between the linear and non-linear image perturbations indicate situations in which we violate the Born approximation. paul1-05.perturbation [CR,M]

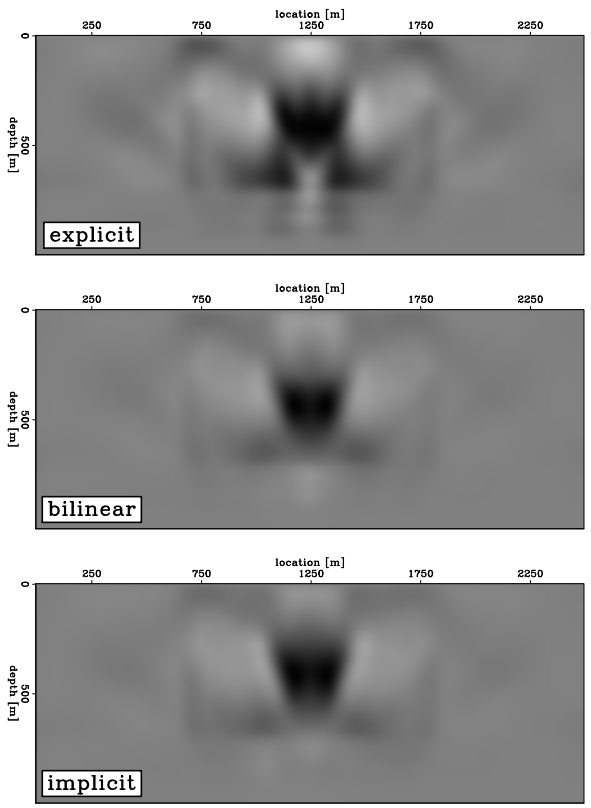

Figure 8: Anomaly of 5%: inversion from the non-linear image perturbation (7) using the explicit (top), bilinear (middle) and implicit (bottom) WEMVA operators. paul1-05.inversion [CR,M]

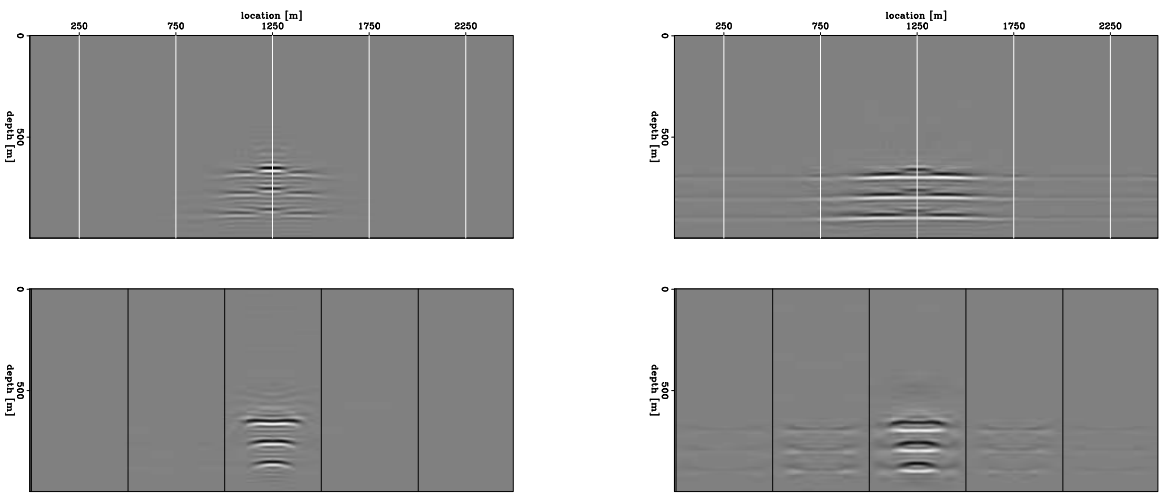

Figure 9: Anomaly of 20%: linear and non-linear image perturbations (left/right); zero offset section (top) and selected angle-gathers (bottom) corresponding to the locations of the vertical lines in the upper panel. Large differences between the linear and non-linear image perturbations indicate situations in which we violate the Born approximation. paul1-20.perturbation [CR,M]

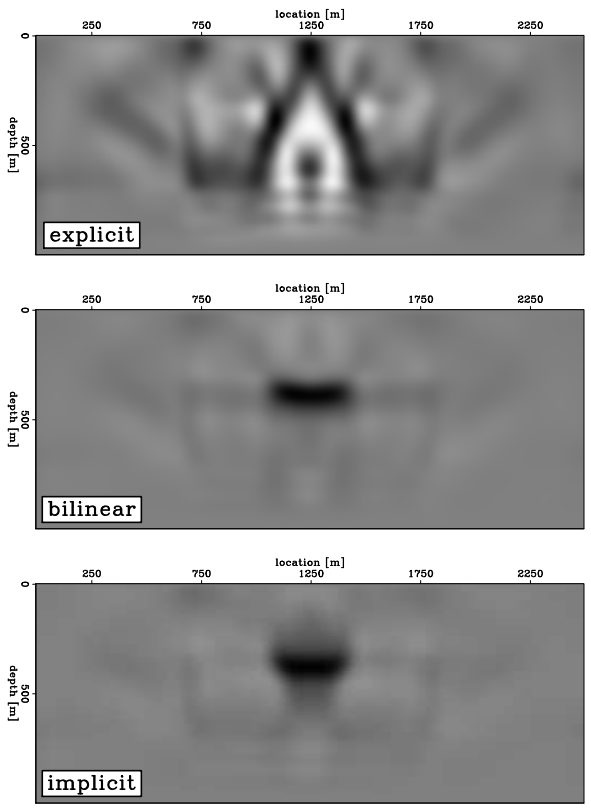

Figure 10: Anomaly of 20%: inversion from the non-linear image perturbation (7) using the explicit (top), bilinear (middle) and implicit (bottom) WEMVA operators. paul1-20.inversion [CR,M]

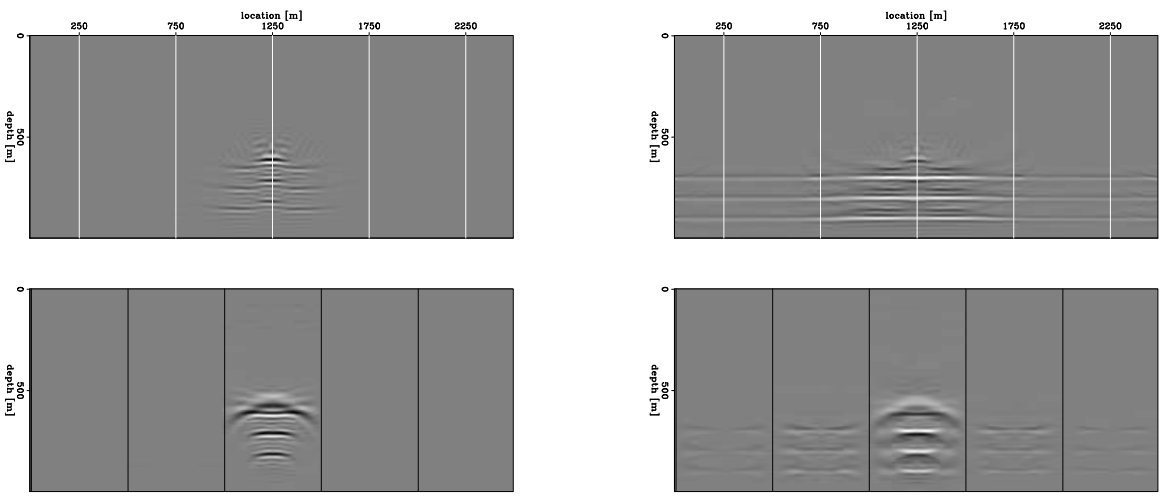

Figure 11: Anomaly of 40%: linear and non-linear image perturbations (left/right); zero offset section (top) and selected angle-gathers (bottom) corresponding to the locations of the vertical lines in the upper panel. Large differences between the linear and non-linear image perturbations indicate situations in which we violate the Born approximation. paul1-40.perturbation [CR,M]

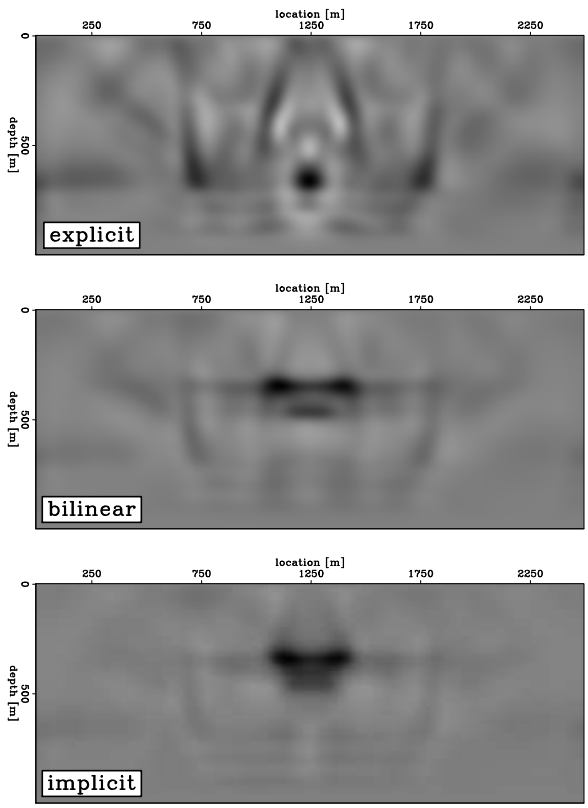

Figure 12: Anomaly of 40%: inversion from the non-linear image perturbation (7) using the explicit (top), bilinear (middle) and implicit (bottom) WEMVA operators. paul1-40.inversion [CR,M]